Crosstalk between SUMOylated PPARγ1 and FOXO1 Exerts a Positive-feedback Effect on Vascular Endothelial Insulin Resistance

Ying Kong
Nanchang University
Ailin Niu
Nanchang University
Wanwan Yuan
Nanchang University
Min Xia
Nanchang University
Xiaowei Xiong
Nanchang University
Yanli Lu
Nanchang University
Tingting Yin
Nanchang University
Yanan Zhang
Nanchang University
Sheng Chen
Nanchang University
Qianqian Huang
Nanchang University
Guohua Zeng
Nanchang University
Qiren Huang (qrhuang@ncu.edu.cn)
Nanchang University https://orcid.org/0000-0002-3434-9484

Original investigation

Keywords: Insulin resistance, Endothelium, PPARγ, SUMOylation, FOXO1, Angiopathy

Posted Date: October 19th, 2021

DOI: https://doi.org/10.21203/rs.3.rs-970766/v1

Abstract

Background: PPARγ and FOXO1 are key regulators of transcription factors that mediate insulin sensitivity. We previously showed that a small ubiquitin-related modifier of PPARγ1 at K77 (SUMOylation) favors endothelial insulin resistance (IR) induced by high-fat/high-glucose (HF/HG) administration. However, whether and how the crosstalk between SUMOylated PPARγ1 and FOXO1 mediates the development of IR remains unclear. Here, we place emphasis on elucidating how PPARγ1-K77 SUMOylation interacts with FOXO1 and participates in the development of endothelial IR.

Methods: Adenovirus or adeno-associated virus carrying a truncated PPARγ1 containing AF1 and DBD domains fused with SUMO-1 (PPARγ1[1-182 aa]-SUMO-1 fusion protein) was utilized to simulate PPARγ1-K77 SUMOylation. Furthermore, we carried out PPARγ1-K77 SUMOylation imitating-IR and worsening-IR experiments *in vitro* and *in vivo.* The vascular diastolic function and levels of p-IKK, IKK, p-PI3K, PI3K, p-Akt, Akt, p-eNOS, and eNOS were measured. To elucidate the underlying mechanism, the interaction of PPARγ1-K77 SUMOylation and FOXO1 was examined by co-immunoprecipitation. The recruitment of PPARγ1 or FOXO1 to PPRE was analyzed by chromatin immunoprecipitation, followed by measuring the PPARγ1 transcriptional activity and translocation of FOXO1.

Results: Our results show that like HF/HG, PPARγ1-K77 SUMOylation imitates endothelial IR and dysfunction, presenting decreased NO levels and elevated ET-1 levels, with PI3K/Akt/eNOS pathway inhibited, and endothelium-dependent vasodilation function impaired. Moreover, combination of HF/HG and PPARγ1-K77 SUMOylation exhibits a synergistic worsening effect on endothelial IR. Mechanistically, the results reveal that PPARγ1-K77 SUMOylation readily interacts with FOXO1, and the PPRE binding site of *PI3K* is competitively blocked by FOXO1, which represses PPARγ1 transcriptional activity and downregulates the PI3K-Akt pathway. Inhibition of the PI3K-Akt pathway promotes the nuclear accumulation of FOXO1, which interacts with SUMOylated PPARγ1 in the nucleus, exerting a positive feedback effect on IR pathogenesis.

Conclusion: These results reveal a novel association between PPARγ1-K77 SUMOylation and FOXO1, which inhibits PPARγ1 transcriptional activity and contributes to vascular endothelial IR. These findings will be beneficial for better understanding the pathogenesis of endothelial IR and providing novel pharmacological targets for diabetic angiopathy.

Introduction

Insulin resistance (IR), a common feature of many metabolic disorders, is referred to as the long-term weak responsiveness of insulin-sensitive target organs or tissues to insulin [1]. Endothelial IR renders the vascular endothelium insensitive to insulin, characterized by a decrease in nitric oxide (NO) secretion and/or an increase in endothelin-1 (ET-1) [2]. Moreover, endothelial IR plays significant pathophysiological roles in cardiovascular diseases, such as atherosclerosis and hypertension, which may be accompanied by endothelial dysfunction [3].

Peroxisome proliferator-activated receptor γ (PPARγ) is a crucial regulator involved in the process of adipocyte differentiation, lipoprotein metabolism, and insulin sensitivity [4]. PPARγ exists as two different isoforms, PPARγ1 and PPARγ2. PPARγ1 is expressed in nearly all cells, including hepatocytes, skeletal muscle cells, vascular cells, cardiomyocytes, and macrophages, while PPARγ2 is highly expressed in adipose tissue. PPARγ enhances insulin sensitivity and adipogenesis through ligand-dependent transcriptional activation. Ligands for this receptor, such as thiazolidinediones (TZDs), have emerged as potent insulin sensitizers and are used in the treatment of hyperglycemia with IR. Unfortunately, TZDs including rosiglitazone and pioglitazone were withdrawn from the market and restricted for use in several countries because of their cardiovascular side effects and increased risk of bladder cancer [5]. Accordingly, the exploration of novel targets and development of new drugs are imminently needed for the amelioration of IR.

Numerous studies in the past decades have indicated that the transcriptional activity of PPARγ is regulated by its posttranslational modifications [6]. Covalent modification of many transcription factors with small ubiquitin-like modifier-1 (SUMO-1) has been identified to engage in trans-activated regulation [7]. PPARγ1 possesses SUMOylation sites at lysine 77 (K77) in the activation function1 (AF1) domain and K365 (murine) in the ligand-binding domain (LBD). In addition, previous studies have reported that SUMOylation of the PPARγ2 AF1 domain at K107 (equivalent to the K77 site of PPARγ1) markedly inhibits PPARγ2 transcription activity *in vitro* and *in vivo* [8]. Another study showed that PPARγ1 SUMOylated at K365 in RAW 264.7 cells, but not at K77, mediated the trans-repression of inflammatory gene promoters by stabilizing the corepressor NCoR/histone deacetylase-3 complex, which is part of a ligand-dependent but PPARγ response element (PPRE)-independent pathway [9]. However, whether SUMOylation of PPARγ1-K77 inhibits PPARγ1 transcriptional activity and contributes to IR in a ligand-independent and PPRE-dependent pattern remains unknown.

Forkhead box O (FOXO) transcription factors include four isoforms, namely FOXO1, FOXO3, FOXO4, and FOXO6, which are expressed in various mammalian cells [10]. Among them, FOXO1 is highly expressed in endothelial cells [11]. In comparison with the aorta endothelia in normal mice, FOXO1 is significantly upregulated in diabetic mice [12]. FOXO1, a canonical regulator of the insulin pathway, has been identified as a downstream target protein of Akt and plays a key role in regulating glucose and lipid metabolism. However, the role of FOXO1 in endothelium IR and its relationship with other transcription factors, such as PPARγ, warrants further investigation. In our previous studies, we found that high-fat and high-glucose (HF/HG) resulted in PPARγ SUMOylation via reactive oxygen species (ROS)-IKK (IκB kinase)-PIAS1 (a specific E3 ligase for PPARγ SUMOylation) pathway in human umbilical vein endothelial cells (HUVECs). SUMOylated PPARγ stabilizes the PPARγ-NCoR complex, leading to endothelial IR [13]. Another study reported that FOXO1 interacts with PPARγ, which represses target gene expression in rat primary adipocytes [14]. Our previous study revealed that a component in green tea, epigallocatechin-3-gallate, inhibited adipocyte differentiation and maturation by negatively regulating FOXO1 phosphorylation via the PI3K-Akt pathway [15].

Our hypothesis is that PPARγ1 SUMOylation at K77 in endothelial cells might crosstalk with FOXO1, contributing to the IR induced by HF/HG. The following questions will be addressed: 1) whether PPARγ1 SUMOylation at K77 simulates and aggravates the IR effect in endothelial cells induced by HF/HG *in vitro* and *in vivo*, and 2) whether SUMOylated PPARγ1 interacts with nuclear transcription factor FOXO1 and how this interaction affects PPARγ1 binding to target gene promoters and ultimately influences the transcriptional activity of PPARγ1.

Materials And Methods

Materials

Adenoviruses carrying PPARγ1(1-182 aa)-SUMO-1, PPARγ1(1-182 aa), and adeno-association viruses carrying Tie2-PPARγ1(1-182 aa)-SUMO-1, Tie2-PPARγ1 (1-182 aa) were constructed and obtained from GeneChem (Shanghai, CHN). Primary antibodies against p-PI3K (Tyr 458), PI3K, p-Akt (Ser 473), Akt, p-eNOS (Ser 1177), eNOS, p-FOXO1 (Ser 256), FOXO1, His-tag, β-actin, and PCNA were purchased from Cell Signalling Technology (MA, USA); antibodies against p-IKKα/β (Ser 176), IKKα/β were from Santa Cruz Biotechnology (CA, USA). Dulbecco's modified Earle's medium (DMEM), radio-immunoprecipitation assay (RIPA) buffer and phenylmethanesulfonyl fluoride (PMSF) was purchased from Solarbio (Beijing, CHN), and foetal bovine serum (FBS) and penicillin-streptomycin were obtained from Gibco (CA, USA). The kits for nitric oxide (NO) assays and ELISA kits for endothelin-1 (ET-1) detection were all purchased from Nanjing Jiancheng Bioengineering Institute (Nanjing, CHN). A kit used for chromatin immunoprecipitation was purchased from Cell Signalling Technology (MA, USA). Recombinant human insulin, acetylcholine (Ach) and sodium nitroprusside (SNP) were purchased from Sigma Aldrich (MO, USA).

Cell culture and establishment of IR model induced by HF/HG *in vitro*

HUVECs were obtained from the American Type Culture Collection (ATCC, Catalogue No. CRL-1730, USA), and primary rat thoracic aorta endothelial cells (RTAECs) were obtained according to a method described in previous studies [16, 17]. Cells were cultured in 100 mm dishes with 5.5 mM low-glucose Dulbecco's modified Earle's medium(L-DMEM) supplemented with 10% fetal bovine serum (FBS) and 1% penicillin-streptomycin (100 U/mL). In additional, heparin (100 μg/mL) as well as endothelial cell growth factor (20 μg/mL) were needed for RTAECs. Cells were cultured in an incubator filled with 5% CO_2 at a humidified atmosphere and a constant temperature at 37 °C.

The IR model was established with HF/HG *in vitro* as described in our previous report with a few improvements [13]. Briefly, the cells were first cultured in DMEM containing 22 mM of glucose and 0.25 mM palmitic acid (PA) for 48 h. Next, they were washed twice with PBS (pH 7.40) and cultured in FBS-free DMEM for 4 h. Subsequently, the cells were treated with 5 mIU/L insulin for 10 min. Finally, the cell

supernatant and cells were harvested for measurements of the levels of nitrite (equivalent to NO) and ET-1, p-PI3K/PI3K, p-Akt/Akt, and p-eNOS/eNOS.

Adenovirus infection in cells and experimental design

The cells infected with adenoviruses carrying a truncation of PPARγ1 (GenBank Accession NM_138711) with intact AF1 domain and a DNA binding domain (DBD) fused with SUMO-1 (GenBank Accession NM_003352), namely Ad-PPARγ1(1-182 aa)-SUMO-1, were used as the PPARγ1-K77 SUMOylation mimic group (Mimic), while the cells infected with PPARγ1(1-182 aa) unfused with SUMO-1, namely Ad-PPARγ1(1-182 aa), were used as the vehicle control group (Veh). The extent of sequence amplification and purification, titer levels, and cell infection were measured according to the instructions provided by GeneChem Technologies, Inc. In the PPARγ1-K77 SUMOylation-imitating IR experiment, HUVECs cultured in either 5.5 mM low-glucose DMEM or 22 mM glucose combined with 0.25 mM PA (22/0.25 mM, HG/HF) for 48 h were respectively considered as the control (Ctrl) or IR group; cells infected with either Ad-PPARγ1(1-182 aa)-SUMO-1 or Ad-PPARγ1(1-182 aa) (MOI=100) and cultured in normal medium for 48 h were used as the SUMOylation mimic (Mimic) or the vehicle (Veh) group, respectively. In the PPARγ1-K77 SUMOylation-worsening IR experiment, treatments in the Ctrl and IR groups were the same as those in the SUMOylation-imitating IR experiment. However, the cells infected with either Ad-PPARγ1(1-182 aa)-SUMO-1 or Ad-PPARγ1(1-182 aa) followed by exposure to HF/HG for 48 h were respectively used as the IR+Mimic or IR+Veh groups. Before evaluated, all these cells were finally stimulated with insulin (5 mIU/L) for 10 min in serum-free medium.

Establishment of IR model *in vivo*

Male SD rats (6-7 weeks old; 180-200 g) were purchased from Nanchang University School of Medicine. All animal procedures were approved by the Institutional Animal Care and Use Committee of Nanchang University School of Medicine and conducted in accordance with the guide for the Care and Use of Laboratory Animals published by the US National Institute of Health (NIH Publication No.85-23, revised 1996). All animals were acclimated to the SPF environment in a 12 h light-dark alternate cycle and approximately 25 °C and 50% humidity and provided with sterilized water. IR was induced by high-fat and high-sucrose (HFS) diets *in vivo*, as described in our previous study with minor modifications [18]. Briefly, after adaptation for 1 week, the rats were fed the HFS diet for 24 weeks. Serum NO and ET-1 levels were tested; protein levels of the PI3K-Akt-eNOS pathway in aortic tissues were measured.

Adeno-associated virus construction and infection and experimental design

AAV9 and the endothelial cell-specific promoter Tie2 were used to construct AAV-Tie2-His-PPARγ1(1-182 aa)-SUMO-1 and AAV-Tie2-His-PPARγ1(1-182 aa). Recombinant virus (1.25×10^{13} v.g.) was diluted in 0.2 mL saline solution and injected into the tail vein of rats. In the PPARγ1-K77 SUMOylation simulating IR experiment, 40 male rats were randomly assigned to the normal group (30 rats) that were fed with regular chow, and the IR group (10 rats), which was fed with HFS diets for 24 weeks. After 24 weeks of feeding, the rats on the regular diet were randomly allocated into control (Ctrl), negative control (Veh), and PPARγ1-K77 SUMOylation mimic (Mimic) groups. The rats in the Mimic group were intravenously infected with AAV-Tie2-His-PPARγ1 [1-182 aa]-SUMO-1, whereas the rats in the Veh group were intravenously infected with AAV-Tie2-His-PPARγ1 [1-182 aa]. After infection, all animals were fed a normal diet for an additional 4 weeks. In the PPARγ1-K77-SUMOylation- worsening IR experiment, in addition to the Ctrl and IR groups, an additional 20 IR-rats were first injected with AAV-Tie2-His-PPARγ1(1-182 aa) (IR+Veh group) or AAV-Tie2-His- PPARγ1(1-182 aa)-SUMO-1 (IR+Mimic group), respectively, and then fed with HFS diets for an additional 24 weeks.

Enzyme-linked immunosorbent assay (ELISA)

The concentrations of ET-1 in rats serum (the total blood column samples with visible hemolysis were excluded) or cell supernatants were detected using a specific ELISA kit. Measurements were performed according to the manufacturer's instructions.

Western blot assay

Cells or aortic tissues isolated from rats were washed three times by pre-cold PBS and lysis buffer was prepared as radio-immunoprecipitation assay (RIPA) buffer supplemented with phenylmethanesulfonyl fluoride (PMSF) (PMSF: RIPA=1:100). Another phosphatase inhibitor cocktail tablet (APPLYGEN, Beijing, CHN) was added for phosphorylation protein detection (1:100). Then, the samples were lysed on ice for 30 min, centrifuged at 14,000 rpm for 15 min at 4 °C, and the supernatants containing total protein were collected immediately for quantification using the BCA protein assay kit (TIANGEN, Beijing, CHN). Equal amounts of protein were loaded and separated on an 8 %–12% SDS-PAGE gel by electrophoresis. The protein samples were transferred onto a polyvinylidene fluoride membrane (Millipore, MA, USA), which was then blocked with 7% skimmed milk solution for 1.5 h, and subsequently incubated at 4 °C overnight with specific primary antibodies at a 1:1000 dilution, under gentle shaking. HRP-conjugated secondary antibody (diluted 1:3000) was incubated for 1 h at room temperature, immunolabeled with an ECL detection kit (FUDE, Hangzhou, CHN) and visualized in the dark. The intensity of the bands was determined using a gel imaging system (Bio-Rad Laboratories, CA, USA), and lanes were quantified using Image J software.

Co-immunoprecipitation assay

Protein samples were prepared for western blot assay, and a suitable quantity of samples was transferred to a new tube as input, and the remaining samples were incubated with the primary antibody under gentle shaking on a rotating shaker at 4 °C overnight. The next day, protein A/G-beads (Millipore) were washed twice with PBS and then added to samples containing antigen-antibody, which was then incubated for 3 h at 4 °C. The beads were washed three times with immunoprecipitation buffer, and the samples were assessed by western blotting.

Immunofluorescence assay

HUVECs were seeded on glass coverslips and treated as previously described. Monolayer cells were first cross-linked with 4% paraformaldehyde for 15 min and then washed three times with PBS. The cells were permeabilized with 0.1% Triton X-100-PBS for 20 min. Next, the samples were blocked with goat serum (Boster, Wuhan, CHN) for 1 h at room temperature, and incubated overnight with rabbit anti-FOXO1 (1:100) at 4 °C under gentle shaking. Following three washes with PBS, the cells were incubated with goat anti-rabbit IgG (H+L) CoraLite 594-conjugated secondary antibody (Proteintech, Wuhan, CHN) for 1 h with gentle shaking. Subsequently, the coverslips were covered with 4, 6-diamidino-2-phenylindole (DAPI) at a final concentration of 1 μg/mL (Solarbio Co., Beijing, CHN) for 5 min for staining. After washing three times with PBS, the slices were covered with slides with a drop of mounting medium. Images were captured at random fields from various areas at 200× magnification using a laser scanning confocal microscope (Olympus, Tokyo, Japan).

Chromatin immunoprecipitation (CHIP) assay

ChIP assay was performed using a commercially available kit, as previously reported [19, 20]. Briefly, 37% formaldehyde was added to the dishes at a final concentration of 1%, followed by incubation for 10 min at 37 °C for protein-DNA cross-linking reaction. The reaction was stopped by supplementation with 125 mM glycine for 5 min at room temperature. After cell sonication, the extracted chromatin was digested and randomly fragmented into 150–900 bp, and the fragments were then incubated overnight at 4 °C with ChIP-grade antibodies against His-tag, FOXO1 (1:50), and IgG, which served as the negative control. Then, ChIP-grade protein G agarose beads were added, and the cross-linked DNA-protein complexes were unlinked to obtain a pure DNA fragment for use as the template for PCR. The following oligonucleotides spanning the putative PI3K-binding site were (F) 5'-TGG TGC ATA CCT GTA GTC CC-3' and (R) 5'-TTT TGA GAT GGA GTC TCG CTT-3'. The bands were obtained by agarose gel electrophoresis. Fold enrichment was calculated by quantitative real-time PCR (q-PCR) to evaluate the degree of PPARγ1 binding to PPRE in the PI3K promoter.

Double luciferase reporter gene assays

For the transactivation assay with a 3×PPRE promoter, HUVECs were seeded on 24-well plates (6×10^4 cells/well), pre-treated as described above, and co-transfected with 250 ng of reporter plasmid (PMCS-*3×PPRE-TK-Luc)* and 25 ng of Renilla plasmid (pRL-TK-Renilla) (10:1), which was regarded as the internal control (GeneChem, Shanghai, CHN), using Lipofectamine 3000 reagent (Invitrogen, CA, USA). Twenty-four hours later, the firefly luciferase and Renilla activities were simultaneously measured using a dual luciferase assay kit (Promega, WI, USA) and quantified using a luminometer. Firefly luciferase activity was normalized to Renilla luciferase activity.

Detection of NO concentrations

The concentrations of NO in the cell supernatants or rats serum (the total blood column samples with visible hemolysis were excluded) were measured using specific kits. The measurements were performed according to the manufacturer's instructions using a microplate reader at the specified optical density.

Detection of vasodilation *in vivo*

Tests were performed as described in previously published studies, with a few modifications [21-24]. Pre-treated rats were anesthetized with 3-4% isoflurane and administered an intraperitoneal injection of 1 U/kg insulin. Another batch of rats was successively injected with acetylcholine (Ach, 0.05 mg/kg) and sodium nitroprusside (SNP, 0.5 mg/kg). Subsequently, the rats were placed in a supine position on a platform with the left neck exposed to the transducer. To obtain better contact between the skin and transducer, a site on the left side of the neck was shaved and gently smeared with ultrasound gel. Subsequently, the left carotid artery was visualized by placing the probe beside the trachea, and images were recorded using an ultrahigh-resolution small animal ultrasound imaging instrument (Vevo 2100, Toronto, CAN). The inner diameter of the left carotid artery (mm) was measured and used for analysis.

Statistical Analysis

All data were expressed as the means ± standard deviation (SD) and analyzed using GraphPad Prism 6.0. Homogeneity of variance and one-way analysis of variance (ANOVA) were determined where appropriate. Comparisons between inner groups were performed using unpaired Student's t-tests. Differences were considered significant if the *P-value* was less than 0.05.

Results

SUMOylation of PPARγ1-K77 simulates and worsens the effect of IR induced by HF/HG *in vitro and in vivo*

To simulate PPARγ1-K77 SUMOylation *in vitro*, a fusion protein vector Ad-PPARγ1(1-182 aa)-SUMO-1 (Mimic) and a vehicle control vector Ad-PPARγ1(1-182 aa) (Veh) were constructed. Ad-PPARγ1(1-182 aa) contains only the K77 SUMOylation site, while the K365 SUMOylation site was excluded (Fig. S1A). As expected, both HUVECs and RTAECs were successfully infected with the viruses (MOI=100, Fig. S1B). Vectors targeting the endothelium AAV-Tie2-His-PPARγ1(1-182 aa) (Veh) and AAV-Tie2-His-PPARγ1 (1-182 aa)-SUMO-1(Mimic) were constructed. The western blot results showed higher expression levels of His-tag in the thoracic aorta tissue than those in other tissues, such as the muscles, liver, and adipose tissue (Fig. S1C and D), suggesting that the AAVs have a strong endothelium-targeting ability.

To observe the effects of PPARγ1-K77 SUMOylation on endothelial IR in response to insulin stimulation, the levels of NO and ET-1 in the supernatant and rat serum were examined. As shown in Fig. 1, the levels of NO in the HF/HG-treated (IR) group were significantly lower than those in the control (Ctrl) group. Likewise, the NO levels in the Mimic group were significantly lower than those in the Veh group (Fig. 1A). In contrast, the ET-1 levels in the IR and Mimic groups were markedly higher than those in the Ctrl and Veh groups, respectively (Fig. 1B). Results from RTAECs were consistent with those from HUVECs (Fig. S2A and B). These data indicate that PPARγ1-K77 SUMOylation simulates HF/HG to induce endothelial IR, along with decreased NO and increased ET-1 levels. Moreover, the levels of NO in the IR+Mimic group were remarkably reduced compared with those in the IR + Veh or IR group, whereas the levels of ET-1 in the IR + Mimic group were significantly increased (Fig. 1C and D), which is consistent with the results from the RTAECs (Fig. S2C and D). Additionally, the results *in vivo* were consistent with the *in vitro* results (Fig. 2A-D). All these data suggest that SUMOylation of PPARγ1 at the K77 site simulates and exacerbates endothelial IR caused by HF/HG.

Since serum NO levels do not completely originate from endothelial eNOS, the inner diameter of the carotid artery was measured using an ultrasonic apparatus to directly evaluate the endothelial response to insulin *in vivo*. After stimulation with insulin, the inner diameter of the rat carotid artery in the IR group was significantly lower than that in the Veh group, and the inner diameter in the Mimic group was markedly smaller than that in the Veh group. In addition, the inner diameter of the carotid artery in the IR+Mimic group was smaller than that in the IR or IR + Veh groups (Fig. 2E and F). Taken together, these data suggest that PPARγ1 SUMOylation at the K77 site imitates and exacerbates the degree of endothelial IR caused by HFS diets.

To further investigate whether PPARγ1-K77 SUMOylation manifests a systemic IR phenotype, we examined the physical and serum biochemical parameters in rats. It was shown that the rats in all these groups had an equivalent body length, but a significant increase in body weight in the IR, IR+Veh, and IR+Mimic groups compared to Ctrl; however, no increase in body weight was observed in the Veh or Mimic groups (Fig. S3A, B, J, K). The rats in the IR group exhibited significant increases in levels of FBG, INS, TC, TG, and HOMA-IR index, as well as the AUC of GTT and ITT, indicating that SUMOylation of PPARγ1-K77 simulates the systemic IR effect induced by the HFS diet (Fig. S3C-I). In addition, as in the IR group, the rats in the IR+Veh group also showed remarkable increases compared with the Ctrl group. However,

the rats in the IR+Mimic group presented more striking elevations compared with the IR+Veh or IR group, demonstrating that SUMOylation of PPARγ1-K77 worsened the systemic IR effect induced by the HFS diet (Fig. S3L-R). These findings indicate that PPARγ1-K77 SUMOylation imitates or further aggravates the IR phenotype caused by HF/HG *in vitro and in vivo*.

PPARγ1-K77 SUMOylation impairs endothelium-dependent vasodilation function

To investigate vascular diastolic function in rats, we used an ultrasound imaging instrument to examine the inner diameter of the carotid artery in response to acetylcholine (Ach) and sodium nitroprusside (SNP). The results indicate that in the Ctrl and Veh groups, the left carotid arteries of rats showed dose-dependent vasodilation in response to Ach; however, this effect was abolished in the IR and Mimic groups. Moreover, the vascular diastolic function of rats in the IR+Mimic group was much worse than that of rats in the IR or IR+Veh group, with no dose-dependent response to Ach (Fig. 3A and B). However, the endothelium-independent vasodilation response induced by SNP did not significantly change among the groups (Fig. 3A and C). These findings indicated that PPARγ1-K77 SUMOylation impaired endothelium-dependent vasodilation function *in vivo*, but the endothelium-independent vasodilation functions were unaffected.

PPARγ1-K77 SUMOylation activates IKK and downregulates PI3K-Akt-eNOS cascade

To further evaluate the effects of PPARγ1-K77 SUMOylation on the insulin pathway, phosphorylation levels of PI3K, Akt, and eNOS were examined after infection with adenoviruses or adeno-associated virus constructs *in vitro* and *in vivo*. The ratio of p-IKK (α/β) to IKK (α/β) in the IR group was remarkably increased compared to that in the Ctrl group. In comparison to the Veh group, there was a significant increase in the p-IKK (α/β) / IKK (α/β) levels in the Mimic group , which was consistent with the results of the comparison between the Ctrl and IR groups (Fig. 4A and B). These results suggest that PPARγ1-K77 SUMOylation activates IKK. We subsequently investigated the effects of PPARγ1-K77 SUMOylation on the PI3K/Akt/eNOS pathway. The phosphorylation levels of PI3K-Akt-eNOS cascades in the IR and Mimic groups were lower than those in the Ctrl or Veh groups (Fig. 4A and C-E). Similar results were obtained from RTAECs (Fig. S4A-E). Moreover, the HUVECs in the IR+Mimic group showed evidently higher phosphorylation levels of IKK and lower phosphorylation levels of PI3K, Akt, and eNOS than those in the IR or IR+Veh group (Fig. 4F-J). These data were further verified in RTAECs (Fig. S4F-J). As expected, the results *in vivo* were consistent with the *in vitro* results (Fig. 5).

PPARγ1 K77 SUMOylation promotes PPARγ1 interaction with FOXO1 and inhibits the transcriptional activity of

PPARγ1

To explore whether PPARγ1-K77 SUMOylation alters the interaction with FOXO1 and affects its transcriptional activity. As shown in Fig. 6A, PPARγ1(1-182 aa)-SUMO-1 presented a stronger ability to interact with FOXO1 than PPARγ1(1-182 aa) unfused SUMO-1. The JASPAR program was used to analyze the PPRE region in the upstream of PI3K promoter. A putative site from -1425 to -1440 bp in the PPRE region was predicted. ChIP assays were conducted to determine whether SUMOylated PPARγ1 at K77 or FOXO1 was recruited to the PPRE site. In both normal and IR states, compared to the Veh group, the SUMOylated-PPARγ1 was less recruited to the PPRE of its target gene PI3K in the Mimic group (Fig. 6B and D). However, a completely opposite recruitment effect was observed for FOXO1 (Fig. 6C and E), indicating that the recruitment of FOXO1 to the PPRE region in the PI3K promoter competitively blocks the recruitment of PPARγ1(1-182 aa) in the Mimic group. To examine the impact of PPARγ1-K77 SUMOylation on its transactivation capacity, reporter gene assays in HUVECs were performed using a luciferase reporter gene driven by a 3×PPRE response element or Renilla linked to the TK promoter. *The relative promoter activity of the Mimic group* was approximately one-third or one-fourth of the level in the Veh group; likewise, the activity of the IR group was about one-fifth that of the Ctrl group (Fig. 6F). Moreover, the activation observed in the IR+Mimic group was lower than that observed in the IR group or IR+Veh group (Fig. 6G), demonstrating that PPARγ1 K77 SUMOylation markedly inhibited the transactivation capacity of PPARγ1.

PPARγ1-K77 SUMOylation modulates the nuclear translocation of FOXO1

To explore how PPARγ1-K77 SUMOylation affected the expression of FOXO1 and its intracellular sub-localization, phosphorylation levels of FOXO1 were first assessed by western blotting. The ratios of p-FOXO1/FOXO1 in the IR and PPARγ1-K77 SUMOylation mimic groups were lower than those in the Ctrl group (Fig. 7A and C).The ratios of p-FOXO1/FOXO1 in the IR+Mimic group were markedly decreased compared to those in the IR or IR+Veh groups (Fig. 7B and D). The effect of PPARγ1-K77 SUMOylation on the translocation of FOXO1 was subsequently determined in nuclear fractions by immunofluorescence staining (Fig. 7E) and western blotting (Fig. 7F) in HUVECs. Compared to the Ctrl or Veh group, HF/HG treatment and PPARγ1-K77 SUMOylation significantly promoted FOXO1 translocation to the nuclei in HUVECs. Moreover, the nuclear expression level of FOXO1 in the IR+Mimic group was markedly higher than that in the IR or IR+Veh group. These findings indicate that PPARγ1-K77 SUMOylation causes FOXO1 nuclear accumulation.

Discussion

IR is a cardiovascular risk factor in the general population, particularly in patients with T2DM [25–28]. Long-term high glucose/fat diet consumption increases the development of IR and promotes the

occurrence of cardiovascular disorders [29, 30]. In the current study, we established an endothelial IR model by combining high-fat with high-glucose treatments *in vivo* and *in vitro*.

Recent studies have shown that SUMOylation of PPARγ may significantly affect its transcriptional activity [31]. Our previous study indicated that hyper-SUMOylation by co-infecting with adenoviruses, including Ad-PPARγ1, Ad-SUMO-1, and Ad-PIAS1, caused vascular endothelial IR in rats [18]. However, off-target effects of PPARγ1 SUMOylation were possible. Therefore, we studied the effects of PPARγ1-K77 SUMOylation on endothelial IR and explored its underlying mechanism by constructing a PPARγ1(1-182 aa)- SUMO-1 fusion protein vector.

Reduced NO production and unaltered or enhanced ET-1 secretion are regarded as the major mechanisms underlying vascular complications [32]. After establishing the IR models, we first used these markers to evaluate the endothelial function. As expected, PPARγ1-K77 SUMOylation markedly decreased NO levels and increased ET-1 levels both *in vitro* and *in vivo*. Importantly, NO production was shown to depend on the phosphorylation of endothelial NO synthase (eNOS) at Ser1177 via the PI3K/Akt pathway [33]. Moreover, NO production is derived from not only eNOS but also iNOS from inflammatory cells; thus, the serum levels of NO may not completely reflect the vasodilation function of endothelial cells.

To evaluate this function intuitively, we observed the vasodilation function of rats in response to Ach and SNP using an ultrasound imaging technique. PPARγ1-K77 SUMOylation not only simulated but also aggravated endothelial dysfunction induced by HFS diet intake in a dose-dependent manner, but the effect of SNP on vasodilatation was unaffected. Notably, Ach targets and acts on vascular endothelial cells to induce the secretion of NO; however, SNP, an NO donor, directly targets VSMCs and triggers endothelium-independent relaxation via the sGC/cGMP pathway [34]. The results further indicated that PPARγ1-K77 SUMOylation impaired endothelium-dependent vascular relaxation and not endothelium-independent vascular relaxation. This was mainly because HFS diet consumption and PPARγ1-K77 SUMOylation disrupted the function of the vascular endothelium to produce NO or reduce NO bioavailability.

PI3K-Akt-eNOS is a classical pathway that regulates NO production in the endothelium [35, 36]. As expected, the phosphorylation levels of PI3K, Akt, and eNOS were markedly decreased in both the IR and mimic groups. Moreover, PPARγ1-K77 SUMOylation followed by HF/HG treatment induced a noticeable decline in the levels of p-PI3K, p-Akt, and p-eNOS *in vitro* and *in vivo*, suggesting that similar to HF/HG treatment, PPARγ1-K77 SUMOylation may negatively regulate the PI3K-Akt-eNOS pathway. IKK is an enzyme complex that activates NF-κB and is involved in the pathogenesis of IR. Moreover, IKKβ directly phosphorylates IRS-1 at Ser307 and impedes the activation of IRS-1, thus negatively regulating the PI3K-Akt pathway [37]. We next investigated whether PPARγ1-K77 SUMOylation, similar to HF/HG treatment, could activate IKK. Interestingly, PPARγ1-K77 SUMOylation markedly increased the phosphorylation levels of IKKα/β and downregulated the PI3K-Akt-eNOS pathway, thus promoting the pathogenesis of IR. However, whether it also promotes the expression of inflammation-related genes (*IL-6, TNF-α*, etc.) associated with IR requires further verification.

Like PPARγ, FOXO1 is also a key nuclear transcription regulator related to the pathogenesis of IR. In the present study, we focused on FOXO1 because information regarding the interaction between PPARγ1-K77 SUMOylation and FOXO1, as well as their effects on endothelium IR, was limited. Accumulating evidence has demonstrated that under physiological conditions, insulin stimulation activates Akt, which in turn inactivates FOXO1 via phosphorylation, alleviating the inhibitory effect of FOXO1 on eNOS. However, in endothelial IR conditions, impaired insulin signaling inhibits the activation of eNOS by de-phosphorylating FOXO1, leading to endothelial dysfunction [38]. Hyperglycemia mediates the nuclear translocation of FOXO1 and enhances its transactivation, which leads to the production of inducible NO and results in endothelial dysfunction [39]. In the current study, the phosphorylation of FOXO1 was significantly decreased, followed by the downregulation of eNOS phosphorylation in HF/HG-treated HUVECs. Moreover, these changes were also observed in the PPARγ1-K77 SUMOylation mimic group, suggesting that PPARγ1-K77 SUMOylation may interact with FOXO1 and participate in the process of endothelial IR. Interestingly, the fusion protein that imitated PPARγ1-K77 SUMOylation could bind to FOXO1 markedly more strongly than unfused SUMO-1. However, the functional domain of PPARγ1 that binds to FOXO1 needs to be determined. In addition, compared with PPARγ1(1-182 aa), which did not fuse with SUMO-1, SUMOylated PPARγ1-K77 was more strongly bound to FOXO1 and failed to be recruited to the PPRE of its target gene *PI3K*. However, a completely opposite recruitment effect was observed for FOXO1, suggesting that FOXO1 may compete with SUMOylated PPARγ1 to bind with the PPRE of its target gene. Moreover, the transcriptional activity of SUMOylated PPARγ1-K77 was decreased under both normal and IR conditions compared to that in the Veh group. Several studies are consistent with the findings of the current study, which indicate that FOXO1 binds to the promoter of PPARγ and represses its transcriptional activity [40]. However, other studies have reported that FOXO1 interacts with PPARγ1 and increases its transcriptional activity in hepatic steatosis [41]. This discrepancy may be due to the different tissues used under various pathological states. Therefore, further studies are essential to verify how FOXO1 regulates the transcriptional activity of PPARγ in other insulin-sensitive tissues, such as skeletal muscle or adipose tissue.

It is widely known that the intracellular sub-localization of FOXO1 is mainly regulated by its post-translational modification (PTM), especially the phosphorylation of FOXO1 at Ser256 [42], which is consistent with our present observations. The current study demonstrated that similar to HF/HG treatment, PPARγ1-K77 SUMOylation inhibited the translocation of FOXO1 from the nucleus to the cytoplasm, which was accompanied by markedly decreasing FOXO1 phosphorylation. Furthermore, these effects were worsened in the HF/HG-treated PPARγ1-K77 SUMOylation mimic group compared to the cells treated with HF/HG alone. It has been demonstrated that elevated intracellular ROS production may activate FOXO1 expression via the JNK pathway. In addition, FOXO1 is retained in the nucleus under oxidative stress conditions [43]. Therefore, we suspected that FOXO1 was translocated from the cytoplasm to the nucleus, not only mediated by the downregulation of the PI3K/Akt pathway but also related to ROS production from HF/HG stimulation. The accumulation of FOXO1 in the nucleus might then facilitate its combination with SUMOylated PPARγ1, thus exerting a synergistic effect on the mechanism underlying IR pathogenesis. Similar to the HF/HG treatment, PPARγ1-K77 SUMOylation might

contribute to vascular oxidative stress and play a role in the pathogenesis of IR. These issues warrant further investigation.

While the current study demonstrated the role of PPARγ1-K77 SUMOylation in the pathogenesis of IR, it has some limitations. We constructed a truncated mutant of PPARγ1 fused with SUMO-1, with forced co-expression of PPARγ1 and SUMO-1 proteins, which might be different from the endogenous covalent modification of SUMO-1 at the K77 site *in vivo*. Thus, this mutant might not represent the function of an intact gene, and this approach might not completely simulate SUMOylation-induced endogenous modification *in vivo*. In addition, whether de-SUMOylation of PPARγ1-K77 SUMOylation could rescue the effect of HF/HG treatment on IR and whether adverse side effects of TZD administration, such as weight gain, could be avoided by using mice homozygous for a mutation (K77R) that prevents SUMOylation at the K77 site needs to be confirmed. There is a need for additional detailed studies in the future to develop a drug that affects PPARγ1 SUMOylation and can be applied for the treatment of IR.

Conclusion

In summary, we demonstrate in the current study that PPARγ1 SUMOylated at the K77 site readily interacts with FOXO1, which blocks the PPRE binding site and inhibits PPARγ transcriptional activity. This negatively regulates the PI3K-Akt pathway and leads to IR. Inhibition of the PI3K-Akt pathway hinders the phosphorylation and translocation of FOXO1, which promotes the interaction of FOXO1 with SUMOylated PPARγ1 in the nucleus, forming a positive feedback and thereby aggravating IR in vascular endothelial cells (Fig. 8). This may provide a new therapeutic strategy for reducing and alleviating diabetic vascular complications.

Abbreviations

Ad: Adenovirus

AAV: Adeno-associated virus

SUMO: Small ubiquitin-like modifier

PPARγ：Peroxisome proliferator-activated receptor-gamma

PPRE: PPARγresponse element

IR: insulin resistance

NO: nitric oxide

ET-1: endothelin-1

Ach: acetylcholine

SNP: sodium nitroprusside

HF/HG: high-fat and high-glucose treatment

HFS: high-fat and high-sucrose diets

SD rats：Sprague-Dawley rats

SPF: specific pathogen free

PI3K: Phosphatidylinositol 3-kinases

Akt: Serine/threonine protein kinase

eNOS: endothelial nitric oxide synthase

FOXO1: Forkhead box O1

IKK: IκB kinase

PA: Palmitic acid

qPCR: Quantitative real-time polymerase chain reaction

T-CHO: Total Cholesterol

TG: Triglyceride

T2DM: Type2 diabetes mellitus

SD: Standard deviation

Declarations

Ethics approval and consent to participate

All animal procedures were approved by the Institutional Animal Care and Use Committee of Nanchang University School of Medicine and conducted in accordance with the guide for the Care and Use of Laboratory Animals published by the US National Institute of Health (NIH Publication No.85-23, revised 1996).

Acknowledgments

This study was supported by the grants from the National Natural Scientific Foundation of China (81960153, 81360060). We are grateful to Dr. Dongyuan Yao and Dr. Lijian Shao for language polishing.

Author Contributions

Ying Kong, Ailin Niu, Wanwan Yuan, Min Xia, Xiaowei Xiong, Yanli Lu performed the research. Qiren Huang and Ying Kong designed the research. Qiren Huang, Ailin Niu, Min Xia, Tingting Yin, Yanan Zhang, Sheng Chen, Guohua Zeng analyzed the data. Qiren Huang and Ying Kong wrote the paper. Qianqian Huang, Wanwan Yuan, Xiaowei Xiong, Guohua Zeng reviewed and edited the paper. All authors read and approved the final manuscript.

Funding

This study was supported by the grants from the National Natural Scientific Foundation of China (81960153, 81360060).

Availability of data and materials

All data and materials are available upon request.

Consent for publication

All authors have declared their consent for this publication.

Competing interests

No potential conflicts of interest relevant to this article were reported.

References

1. Riehle C, Abel ED. Insulin signaling and heart failure. Circ Res. 2016;118(7):1151–69. https://doi.org/10.1161/circresaha.116.306206.
2. Muniyappa R, Chen H, Montagnani M, Sherman A, Quon MJ. Endothelial dysfunction due to selective insulin resistance in vascular endothelium: insights from mechanistic modeling. Am J Physiol Endocrinol Metab. 2020;319(3):E629–46. https://doi.org/10.1152/ajpendo.00247.2020.
3. Kim JA, Montagnani M, Koh KK, Quon MJ. Reciprocal relationships between insulin resistance and endothelial dysfunction: molecular and pathophysiological mechanisms. Circulation. 2006;113(15):1888–904. https://doi.org/10.1161/circulationaha.105.563213.
4. Janani C, Ranjitha Kumari BD. PPAR gamma gene–a review. Diabetes Metab Syndr. 2015;9(1):46–50. https://doi.org/10.1016/j.dsx.2014.09.015.

5. Riess ML, Elorbany R, Weihrauch D, Stowe DF, Camara AKS. PPARγ-independent side effects of thiazolidinediones on mitochondrial redox state in rat isolated hearts. Cells 2020, 9(1). https://doi.org/10.3390/cells9010252.
6. Brunmeir R, Xu F. Functional regulation of PPARs through post-translational modifications. Int J Mol Sci 2018, 19(6). https://doi.org/10.3390/ijms19061738.
7. Chung SS, Ahn BY, Kim M, Kho JH, Jung HS, Park KS. SUMO modification selectively regulates transcriptional activity of peroxisome-proliferator-activated receptor γ in C2C12 myotubes. Biochem J. 2011;433(1):155–61. https://doi.org/10.1042/bj20100749.
8. Katafuchi T, Holland WL, Kollipara RK, Kittler R, Mangelsdorf DJ, Kliewer SA. PPARγ-K107 SUMOylation regulates insulin sensitivity but not adiposity in mice. Proc Natl Acad Sci U S A. 2018;115(48):12102–11. https://doi.org/10.1073/pnas.1814522115.
9. Pascual G, Fong AL, Ogawa S, Gamliel A, Li AC, Perissi V, Rose DW, Willson TM, Rosenfeld MG, Glass CK. A SUMOylation-dependent pathway mediates transrepression of inflammatory response genes by PPAR-gamma. Nature. 2005;437(7059):759–63. https://doi.org/10.1038/nature03988.
10. Lee S, Dong HH. FoxO integration of insulin signaling with glucose and lipid metabolism. J Endocrinol. 2017;233(2):R67-r79. https://doi.org/10.1530/joe-17-0002.
11. Wilhelm K, Happel K, Eelen G, Schoors S, Oellerich MF, Lim R, Zimmermann B, Aspalter IM, Franco CA, Boettger T, et al. FOXO1 couples metabolic activity and growth state in the vascular endothelium. Nature. 2016;529(7585):216–20. https://doi.org/10.1038/nature16498.
12. Cifarelli V, Lee S, Kim DH, Zhang T, Kamagate A, Slusher S, Bertera S, Luppi P, Trucco M, Dong HH. FOXO1 mediates the autocrine effect of endothelin-1 on endothelial cell survival. Mol Endocrinol. 2012;26(7):1213–24. https://doi.org/10.1210/me.2011-1276.
13. Lan D, Shen X, Yuan W, Zhou Y, Huang Q. Sumoylation of PPARγ contributes to vascular endothelium insulin resistance through stabilizing the PPARγ-NcoR complex. J Cell Physiol. 2019;234(11):19663–74. https://doi.org/10.1002/jcp.28567.
14. Armoni M, Harel C, Karni S, Chen H, Bar-Yoseph F, Ver MR, Quon MJ, Karnieli E. FOXO1 represses peroxisome proliferator-activated receptor-gamma1 and -gamma2 gene promoters in primary adipocytes. A novel paradigm to increase insulin sensitivity. J Biol Chem. 2006;281(29):19881–91. https://doi.org/10.1074/jbc.m600320200.
15. Lu Y, Chen J, Xian T, Zhou Y, Yuan W, Wang M, Gan Y, Wang K, Xiong S, Ma C, et al. Epigallocatechin-3-gallate suppresses differentiation of adipocytes via regulating the phosphorylation of FOXO1 mediated by PI3K-AKT signaling in 3T3-L1 cells. Oncotarget. 2018;9(7):7411–23. https://doi.org/10.18632/oncotarget.23590.
16. Tian H, Suo N, Li F, Yang CL, Qiong X. An effective method of isolating endothelial cells from intact rat aorta. Cell Biochem Biophys. 2014;70(1):423–7. https://doi.org/10.1007/s12013-014-9933-4.
17. Zhang Z, Li K. Curcumin attenuates high glucose-induced inflammatory injury through the reactive oxygen species-phosphoinositide 3-kinase/protein kinase B-nuclear factor-κB signaling pathway in

rat thoracic aorta endothelial cells. J Diabetes Investig. 2018;9(4):731–40. https://doi.org/10.1111/jdi.12767.

18. Yuan W, Ma C, Zhou Y, Wang M, Zeng G, Huang Q. Negative regulation of eNOS-NO signaling by over-SUMOylation of PPARγ contributes to insulin resistance and dysfunction of vascular endothelium in rats. Vascul Pharmacol. 2019;122-123::106597. https://doi.org/10.1016/j.vph.2019.106597.
19. Wang JD, Cao YL, Li Q, Yang YP, Jin M, Chen D, Wang F, Wang GH, Qin ZH, Hu LF, et al. A pivotal role of FOS-mediated BECN1/Beclin 1 upregulation in dopamine D2 and D3 receptor agonist-induced autophagy activation. Autophagy. 2015;11(11):2057–73. https://doi.org/10.1016/j.vph.2019.106597.
20. Kim YJ, Kim HJ, Chung KY, Choi I, Kim SH. Transcriptional activation of PIK3R1 by PPARγ in adipocytes. Mol Biol Rep. 2014;41(8):5267–72. https://doi.org/10.1007/s11033-014-3398-9.
21. Meng Z, Li J, Zhang Q, Bai W, Yang Z, Zhao Y, Wang F. Vasodilator effect of gaseous sulfur dioxide and regulation of its level by Ach in rat vascular tissues. Inhal Toxicol. 2009;21(14):1223–8. https://doi.org/10.3109/08958370902798463.
22. Razuvaev A, Lund K, Roy J, Hedin U, Caidahl K. Noninvasive real-time imaging of intima thickness after rat carotid artery balloon injury using ultrasound biomicroscopy. Atherosclerosis. 2008;199(2):310–6. https://doi.org/10.1016/j.atherosclerosis.2007.11.035.
23. Ragginer C, Bernecker C, Ainoedhofer H, Pailer S, Kieslinger P, Truschnig-Wilders M, Gruber HJ. Treatment with the nitric oxide donor SNP increases triiodothyronine levels in hyper- and hypothyroid Sprague-Dawley rats. Horm Metab Res. 2013;45(11):808–12. https://doi.org/10.1055/s-0033-1349892.
24. Wu J, Zhang H, Zheng H, Jiang Y. Hepatic inflammation scores correlate with common carotid intima-media thickness in rats with NAFLD induced by a high-fat diet. BMC Vet Res. 2014;10:162. https://doi.org/10.1186/1746-6148-10-162.
25. Adeva-Andany MM, Martínez-Rodríguez J, González-Lucán M, Fernández-Fernández C, Castro-Quintela E. Insulin resistance is a cardiovascular risk factor in humans. Diabetes Metab Syndr. 2019;13(2):1449–55. https://doi.org/10.1016/j.dsx.2019.02.023.
26. Sampath Kumar A, Maiya AG, Shastry BA, Vaishali K, Ravishankar N, Hazari A, Gundmi S, Jadhav R. Exercise and insulin resistance in type 2 diabetes mellitus: a systematic review and meta-analysis. Ann Phys Rehabil Med. 2019;62(2):98–103. https://doi.org/10.1016/j.rehab.2018.11.001.
27. DeFronzo RA, Ferrannini E, Groop L, Henry RR, Herman WH, Holst JJ, Hu FB, Kahn CR, Raz I, Shulman GI, et al. Type 2 diabetes mellitus. Nat Rev Dis Primers. 2015;1:15019. https://doi.org/10.1038/nrdp.2015.19.
28. Arneth B, Arneth R, Shams M. Metabolomics of type 1 and type 2 diabetes. Int J Mol Sci 2019, 20(10). https://doi.org/10.3390/ijms20102467.
29. Small L, Brandon AE, Turner N, Cooney GJ. Modeling insulin resistance in rodents by alterations in diet: what have high-fat and high-calorie diets revealed? Am J Physiol Endocrinol Metab. 2018;314(3):E251–65. https://doi.org/10.1152/ajpendo.00337.2017.

30. Pan Y, Rong Y, Huang J, Zhu K, Chen J, Yu C, Chen M. Lower cardiovagal tone and baroreflex sensitivity associated with hepatic insulin resistance and promote cardiovascular disorders in Tibetan minipigs induced by a high fat and high cholesterol diet. J Diabetes Complications. 2019;33(4):278–88. https://doi.org/10.1016/j.jdiacomp.2018.12.014.
31. Ohshima T, Koga H, Shimotohno K. Transcriptional activity of peroxisome proliferator-activated receptor gamma is modulated by SUMO-1 modification. J Biol Chem. 2004;279(28):29551–7. https://doi.org/10.1074/jbc.m403866200.
32. Artunc F, Schleicher E, Weigert C, Fritsche A, Stefan N, Häring HU. The impact of insulin resistance on the kidney and vasculature. Nat Rev Nephrol. 2016;12(12):721–37. https://doi.org/10.1038/nrneph.2016.145.
33. Symons JD, McMillin SL, Riehle C, Tanner J, Palionyte M, Hillas E, Jones D, Cooksey RC, Birnbaum MJ, McClain DA, et al. Contribution of insulin and Akt1 signaling to endothelial nitric oxide synthase in the regulation of endothelial function and blood pressure. Circ Res. 2009;104(9):1085–94. https://doi.org/10.1161/circresaha.108.189316.
34. Newcomer SC, Taylor JC, McAllister RM, Laughlin MH. Effects of chronic nitric oxide synthase inhibition on endothelium-dependent and -independent relaxation in arteries that perfuse skeletal muscle of swine. Endothelium. 2008;15(1):17–31. https://doi.org/10.1080/10623320802092211.
35. Li CY, Wang LX, Dong SS, Hong Y, Zhou XH, Zheng WW, Zheng C. Phlorizin exerts direct protective effects on palmitic acid (PA)-induced endothelial dysfunction by activating the PI3K/AKT/eNOS signaling pathway and increasing the levels of nitric oxide (NO). Med Sci Monit Basic Res. 2018;24:1–9. https://doi.org/10.12659/msmbr.907775.
36. Yu S, Wong SL, Lau CW, Huang Y, Yu CM. Oxidized LDL at low concentration promotes in-vitro angiogenesis and activates nitric oxide synthase through PI3K/Akt/eNOS pathway in human coronary artery endothelial cells. Biochem Biophys Res Commun. 2011;407(1):44–8. https://doi.org/10.1016/j.bbrc.2011.02.096.
37. Zand H, Morshedzadeh N, Naghashian F. Signaling pathways linking inflammation to insulin resistance. Diabetes Metab Syndr. 2017;11(Suppl 1):307-s309. https://doi.org/10.1016/j.dsx.2017.03.006.
38. Karki S, Farb MG, Ngo DT, Myers S, Puri V, Hamburg NM, Carmine B, Hess DT, Gokce N. Forkhead box O-1 modulation improves endothelial insulin resistance in human obesity. Arterioscler Thromb Vasc Biol. 2015;35(6):1498–506. https://doi.org/10.1161/atvbaha.114.305139.
39. Benchoula K, Arya A, Parhar IS, Hwa WE. FoxO1 signaling as a therapeutic target for type 2 diabetes and obesity. Eur J Pharmacol. 2021;891:173758. https://doi.org/10.1016/j.ejphar.2020.173758.
40. Dowell P, Otto TC, Adi S, Lane MD. Convergence of peroxisome proliferator-activated receptor gamma and Foxo1 signaling pathways. J Biol Chem. 2003;278(46):45485–91. https://doi.org/10.1074/jbc.m309069200.
41. Kim DH, Ha S, Choi YJ, Dong HH, Yu BP, Chung HY. Altered FoxO1 and PPARγ interaction in age-related ER stress-induced hepatic steatosis. Aging. 2019;11(12):4125–44.

https://doi.org/10.18632/aging.102042.

42. Chen J, Lu Y, Tian M, Huang Q. Molecular mechanisms of FOXO1 in adipocyte differentiation. J Mol Endocrinol. 2019;62(3):R239-r253. https://doi.org/10.1530/jme-18-0178.
43. Kawamori D, Kaneto H, Nakatani Y, Matsuoka TA, Matsuhisa M, Hori M, Yamasaki Y. The forkhead transcription factor Foxo1 bridges the JNK pathway and the transcription factor PDX-1 through its intracellular translocation. J Biol Chem. 2006;281(2):1091–8. https://doi.org/10.1074/jbc.m508510200.

Figures

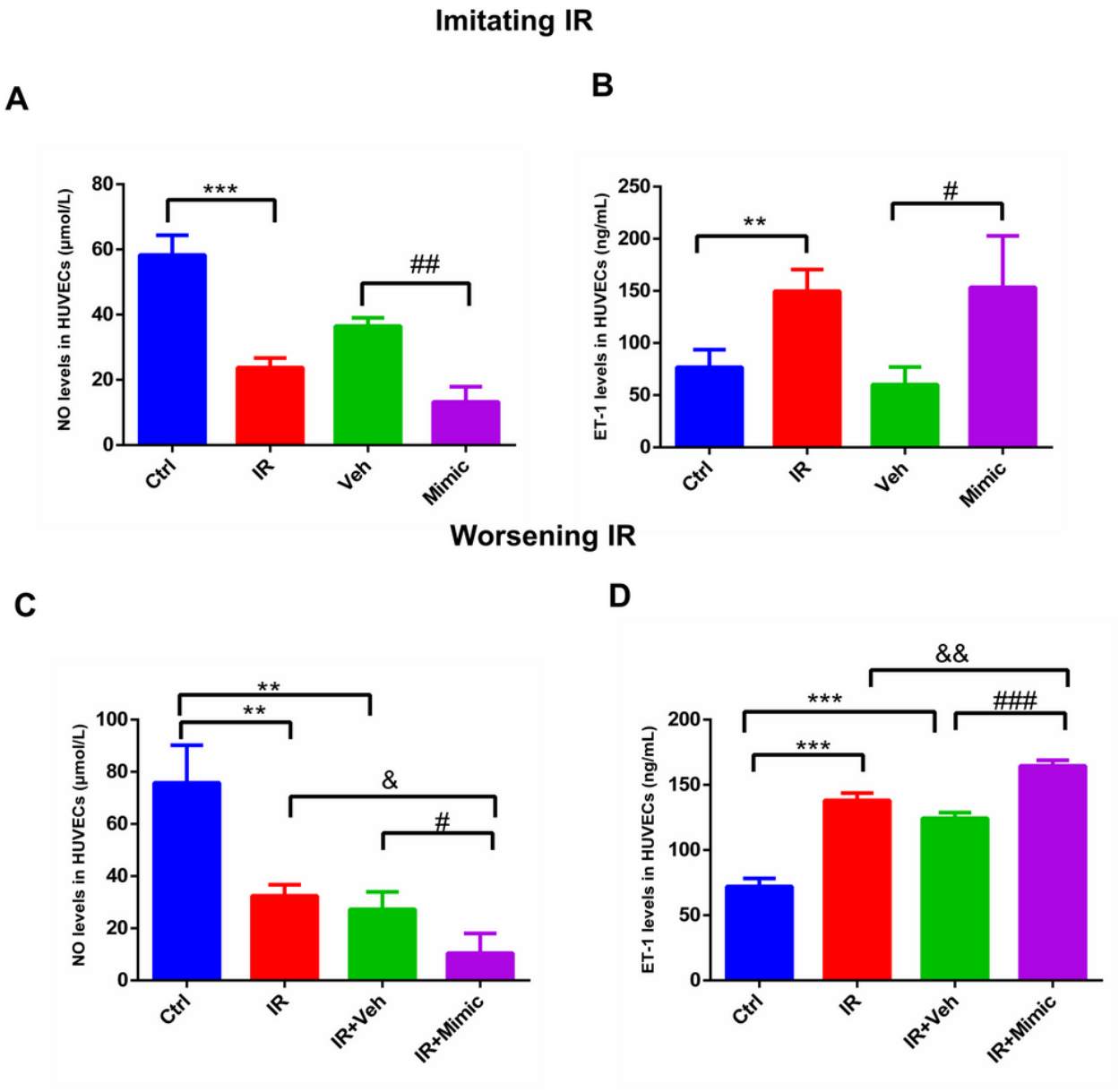

Figure 1

SUMOylation of PPARγ1 at the K77 site results in IR in HUVECs. A-D: Changes in NO and ET-1 levels induced by PPARγ1-K77 SUMOylation imitating (A, B) and worsening IR (C, D) in HUVECs. All the data are expressed as mean ± SD of 3 independent experiments. **P<0.01, and ***P<0.001 vs. the Ctrl group; #P<0.05, ##P<0.01, and ###P<0.001 vs. Veh or IR+Veh group; &P<0.05, and &&P<0.01 vs. IR group.

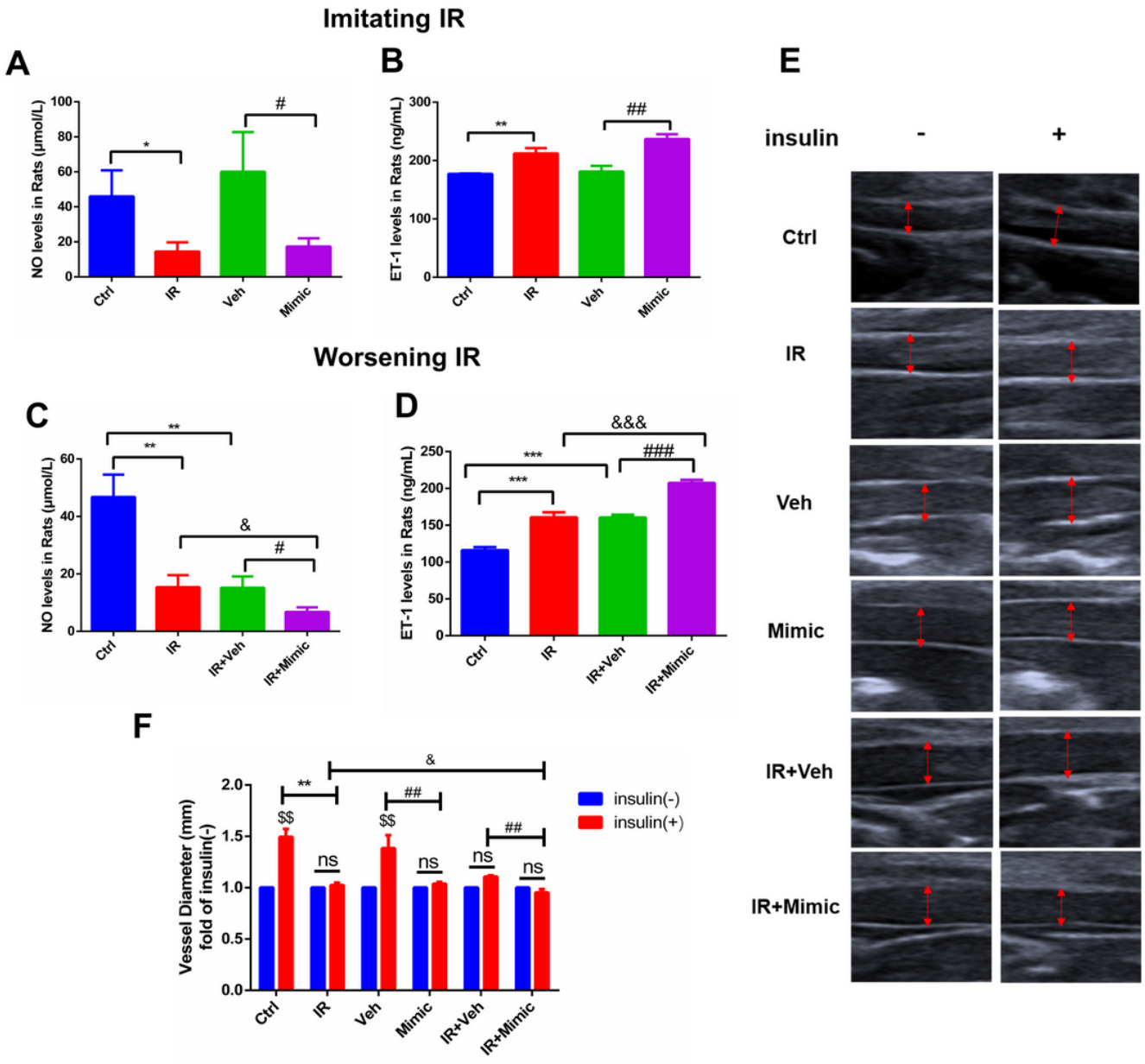

Figure 2

PPARγ1-K77 SUMOylation mimics or aggravates the endothelial IR in rats. A-D: changes in serum NO and ET-1 levels induced by PPARγ1-K77 SUMOylation imitating (A and B) and worsening IR (C and D) in rats. E and F: inner diameters of the carotid artery induced by PPARγ1-K77 SUMOylation imitating and worsening IR in the rat. All the data are expressed as the mean ± SD of 3 independent experiments. *P<0.05, **P<0.01, and ***P<0.001 vs. the Ctrl group; #P<0.05, ##P<0.01, and ###P<0.001 vs. the Veh or

IR+Veh group; &P<0.05 and &&&P<0.001 vs. the IR group; $$P<0.01, or ns (no significance) vs. the groups without insulin.

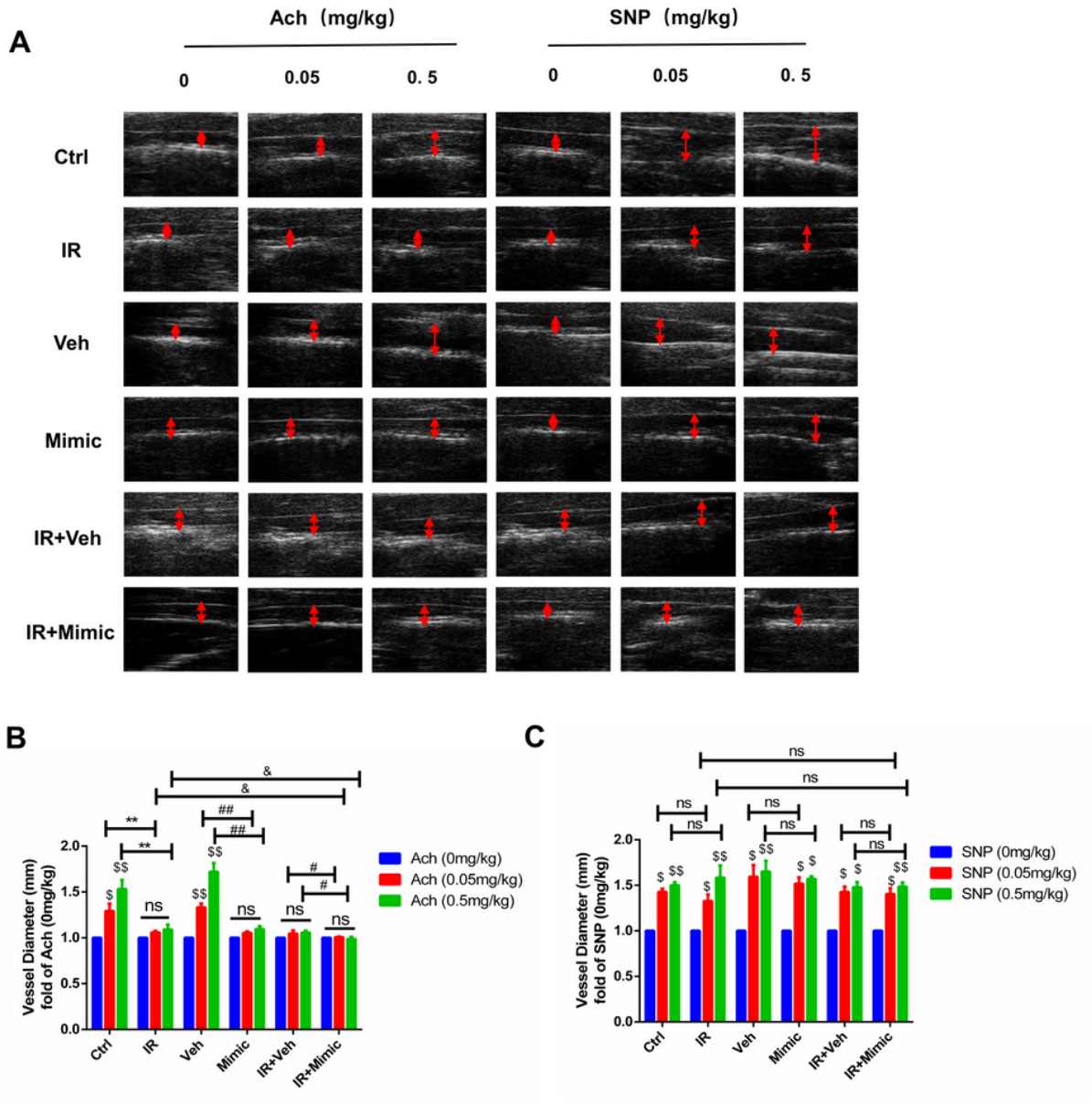

Figure 3

PPARγ1-K77 SUMOylation impairs endothelium-dependent vasodilation in vivo. A-C: the inner diameters of the left carotid artery in the presence of various concentrations of Ach (A and B) and SNP (i.p.) (A and C) were shown. All data are expressed as the mean ± S.D. of 6 rats. **P<0.01 vs. Ctrl group; #P<0.05, and ##P<0.01 vs. Veh or IR+Veh group;&P<0.05 vs. IR group; $P<0.05, and $$P<0.01 vs. 0 mg/kg group. ns: no significance.

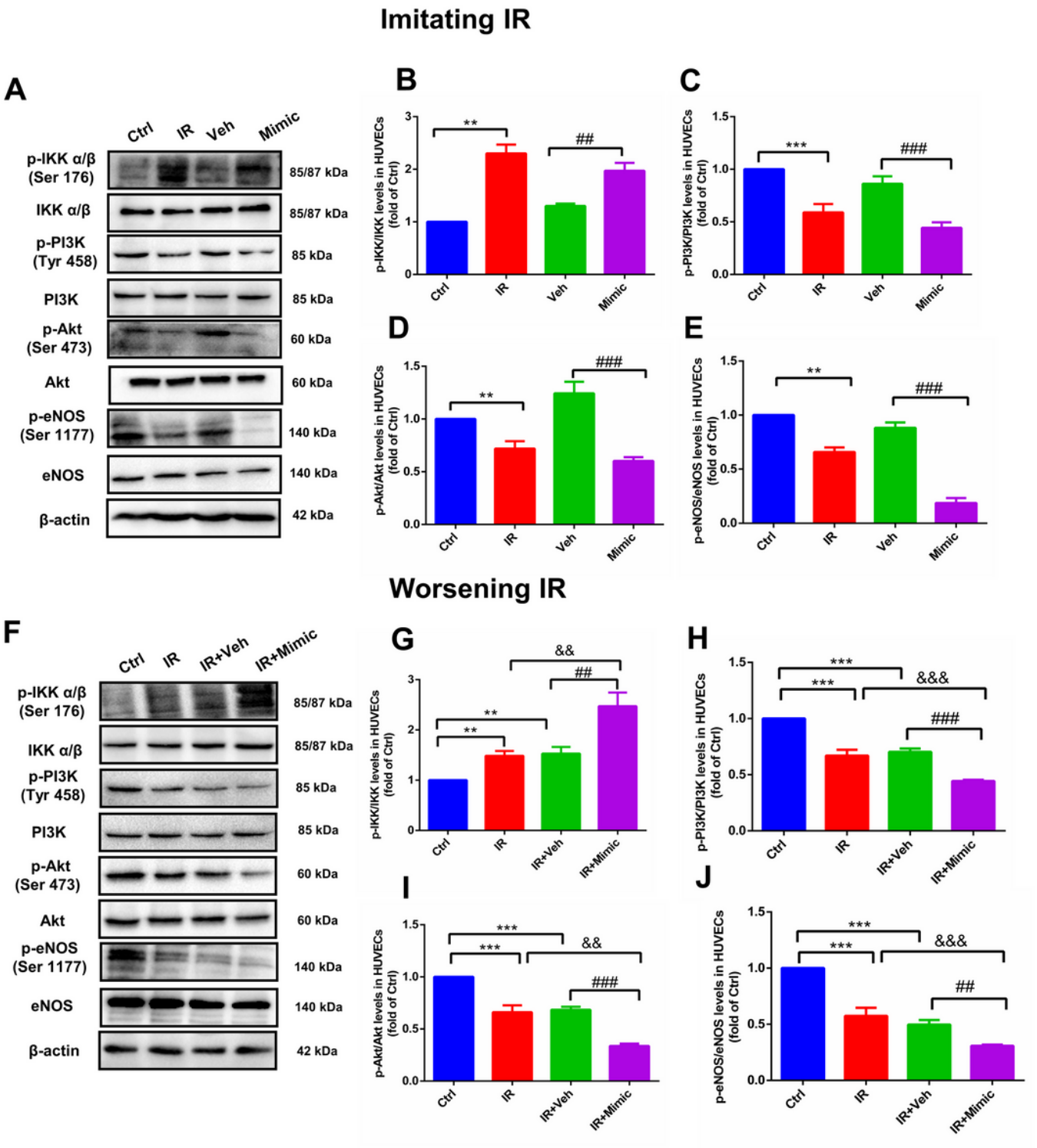

Figure 4

PPARγ1-K77 SUMOylation activates IKK and inhibits PI3K-Akt-eNOS pathway in HUVECs. To investigate the IR imitating and worsening effects of PPARγ1-K77 SUMOylation, A-J: representative western blot bands and the expression analysis for p-IKK/IKK (A, B and F, G), p-PI3K/PI3K (A, C and F, H), p-Akt/Akt (A, D and F, I) as well as p-eNOS/eNOS (A, E and F, J) were shown. All the data are expressed as mean ± SD

of 3 independent experiments. **P<0.01, and ***P<0.001 vs. the Ctrl group; ##P<0.01, and ###P<0.001 vs. the Veh or IR+Veh group; &&P<0.01, and &&&P<0.001 vs. the IR group.

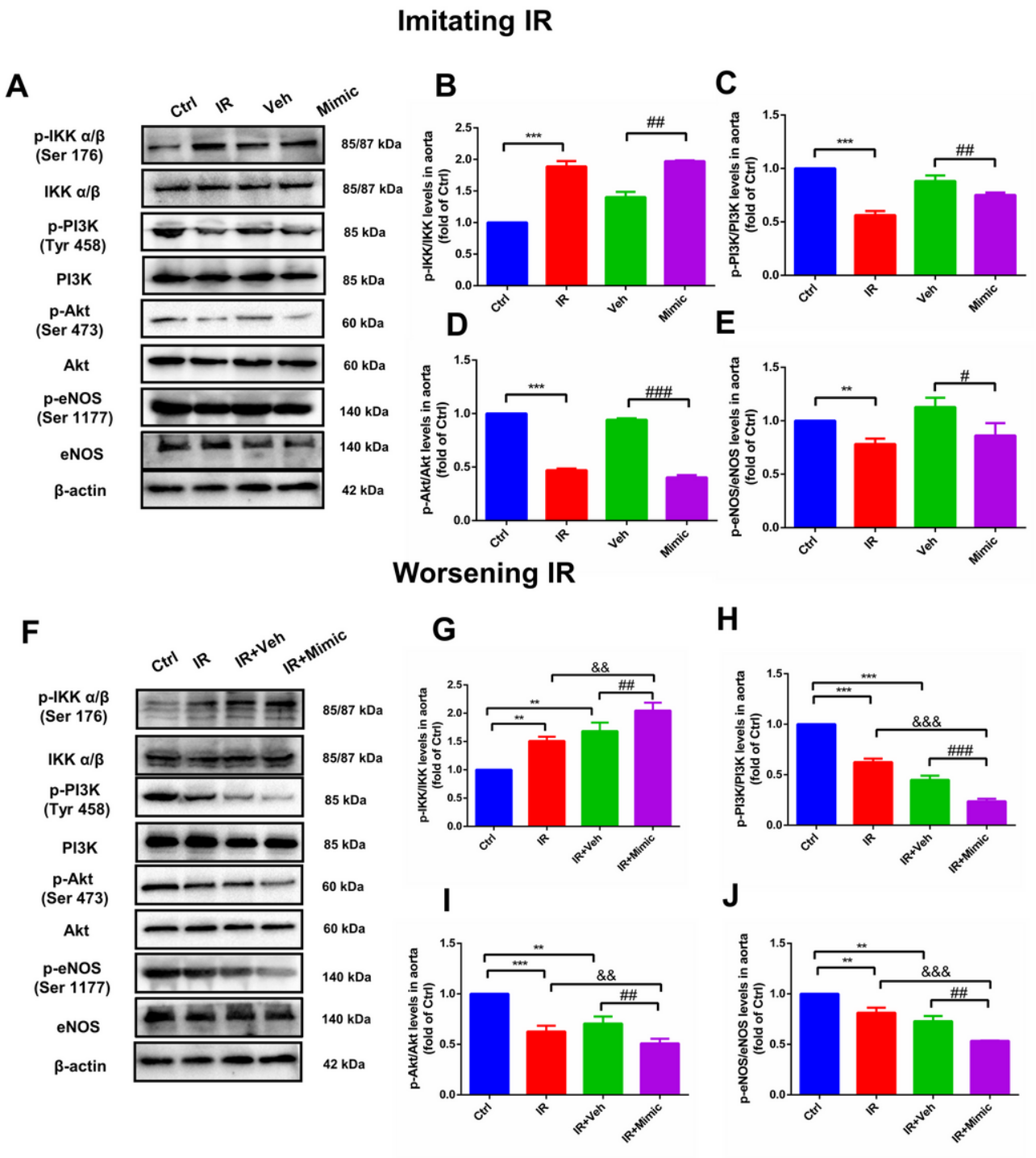

Figure 5

PPARγ1-K77 SUMOylation activates IKK and inhibits PI3K-Akt-eNOS pathway in rats. To investigate the IR imitating and worsening effects of PPARγ1-K77 SUMOylation in the rat, A-J: representative western blot bands and the expression analysis for p-IKK/IKK (A, B and F, G), p-PI3K/PI3K (A, C and F, H), p-Akt/Akt (A, D and F, I) as well as p-eNOS/eNOS (A, E and F, J) were shown. All the data are expressed as the mean ±

SD of 3 independent experiments. **P<0.01, and ***P<0.001 vs. the Ctrl group; #P<0.05, ##P<0.01, and ###P<0.001 vs. the Veh or IR+Veh group; &&P<0.01, and &&&P<0.001 vs. the IR group.

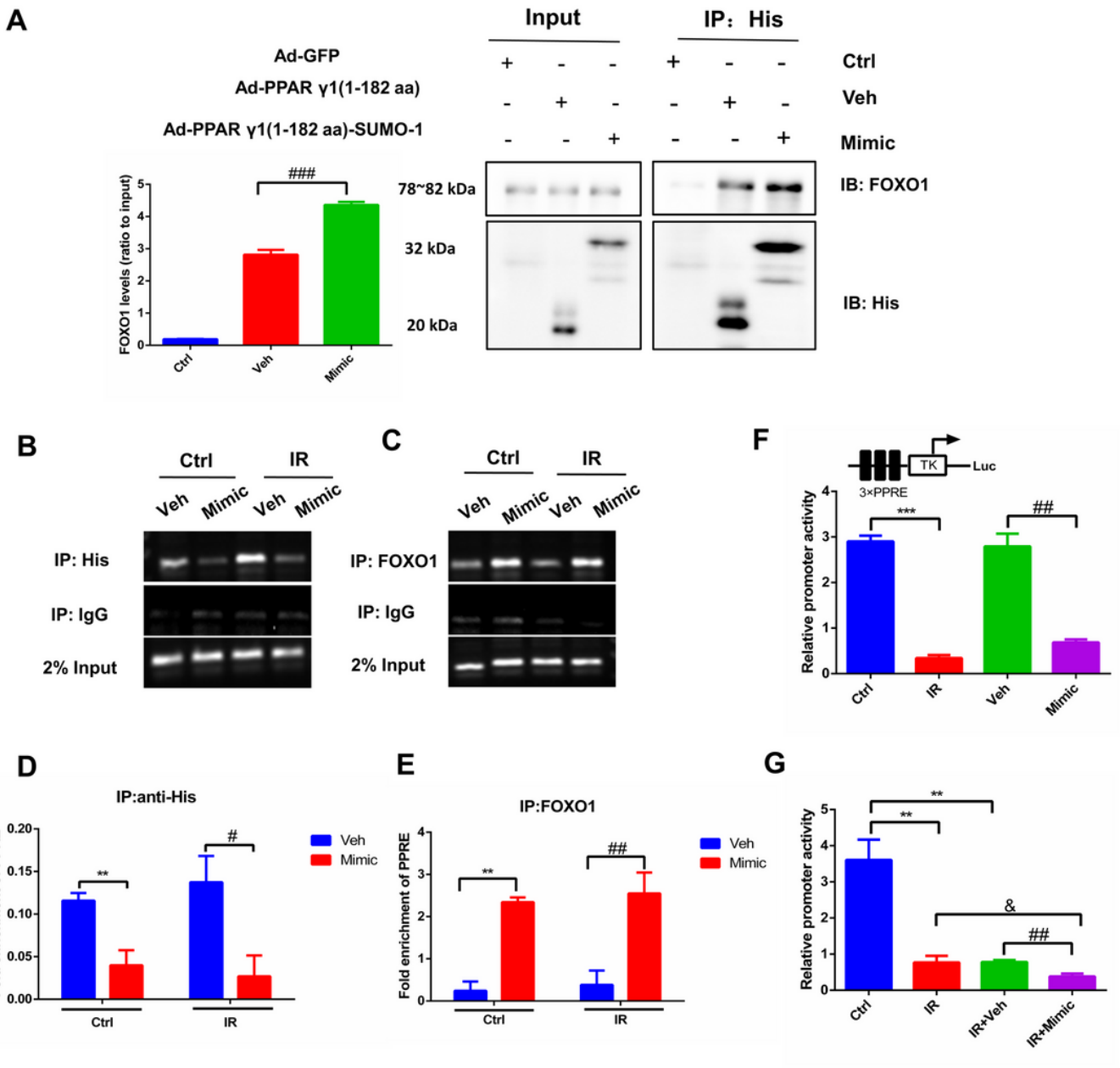

Figure 6

PPARγ1-K77 SUMOylation interacts with FOXO1 and represses the transcriptional activity of PPARγ1. A: PPARγ1-K77 SUMOylation promotes its binding with endogenous FOXO1 as demonstrated by Co-IP assays. B and C: a 150 bp region of the human PI3K promoter was amplified spanning the PPRE sequence by CHIP assay. D and E: CHIP-qPCR assay analysis indicates that PPARγ1-K77 SUMOylation is required for FOXO1 recruitment to the promoter of the target gene PI3K under both normal and IR conditions. F and G: HUVECs were co-transfected with TK-PPRE×3-Luc and Renilla-Luc. Firefly and Renilla luciferase activities were detected for PPARγ1-K77 SUMOylation imitating (F) and worsening IR (G). All

the data are expressed as the mean ± SD of 3 independent experiments. **P<0.01, and ***P<0.001 vs. the Ctrl group; #P<0.05, ##P<0.01, ###P<0.001 vs. the Veh or IR+Veh group; &P<0.05 vs. the IR group.

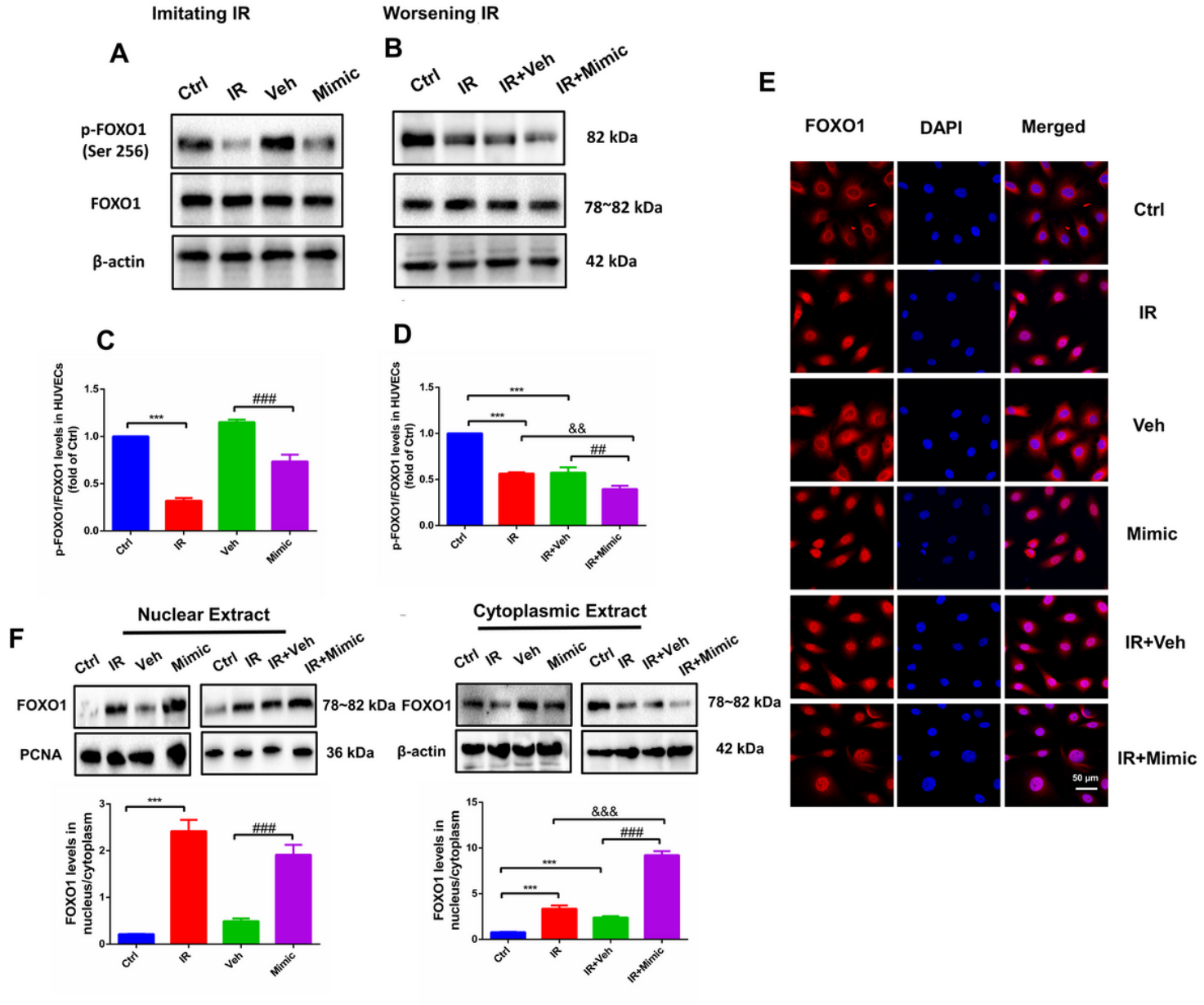

Figure 7

PPARγ1-K77 SUMOylation affects FOXO1 translocation. A-D: representative western blot bands and the expression analysis for p-FOXO1/FOXO1 to investigate the IR imitating (A and C) and worsening (B and D) effects of PPARγ1-K77 SUMOylation in HUVECs. E: the sub-localization of FOXO1 in HUVECs was assessed by immunofluorescent staining; panels show FOXO1 (red), DAPI (blue), and merged signals obtained by confocal microscopy (×200). F: nuclear and cytoplasmic extracts from HUVECs were subjected to western blotting to detect the expression of FOXO1, and the nucleus/cytoplasm ratio of FOXO1 was measured. Results are expressed as mean ± SD (n=3). ***P<0.001 vs. Ctrl group; ##P<0.01, ###P< 0.001 vs. the Veh or IR+Veh group; &&P<0.01, and &&&P<0.001 vs. IR group. Scale bar: 50 μm.

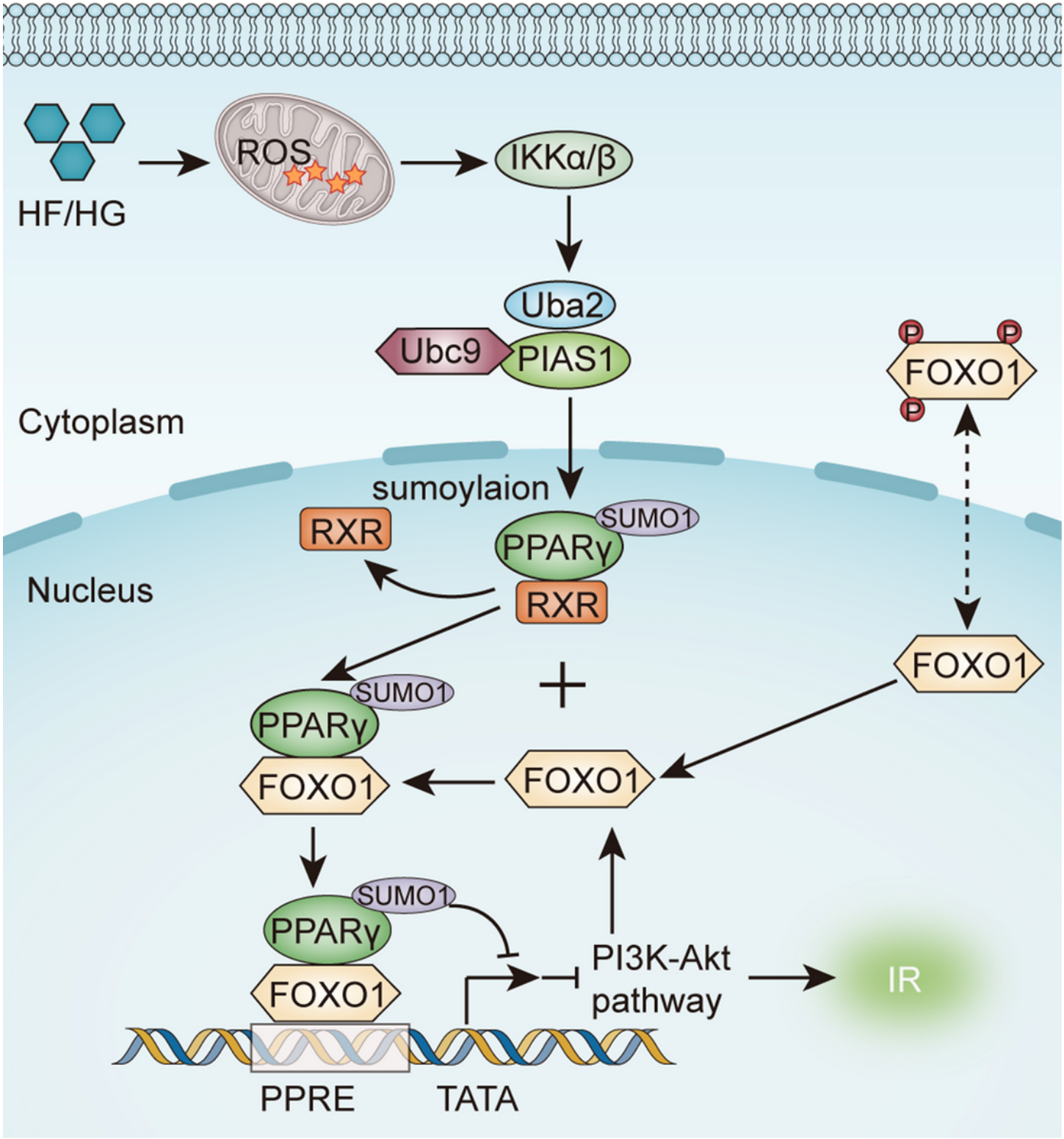

Figure 8

Hypothesis of the interaction between SUMOylated PPARγ1 and FOXO1 exerting positive feedback effects on IR. The crosstalk between PPARγ1-K77 SUMOylation and FOXO1 inhibits PPARγ1 transcriptional activity and negatively regulates the PI3K-Akt pathway. Inhibition of the PI3K-Akt pathway leads to the nuclear accumulation of FOXO1, which promotes the interaction of FOXO1 with SUMOylated

PPARγ1 in the nucleus, forming a positive feedback and thereby aggravating IR in vascular endothelial cells.

Supplementary Files

This is a list of supplementary files associated with this preprint. Click to download.

- Fig.S1.tif
- Fig.S2.tif
- Fig.S3.tif
- Fig.S4.tif
- SupplementaryMaterial.doc